AGU100 ADVANCING EARTH AND SPACE SCIENCE

JGR

Journal of Geophysical Research: Space Physics

RESEARCH ARTICLE

10.1029/2017JA024926

Key Points:

- A theoretical model of spacecraft-charging mitigation for the emission of a relativistic electron beam by a magnetospheric spacecraft is presented
- The model is in good agreement with particle-in-cell simulations
- The model predicts the long-time value of the spacecraft potential, indicating that a relativistic beam would be easily emitted

Supporting Information:

- Supporting Information S1
- Data Set S1

Correspondence to:
G. L. Delzanno,
delzanno@lanl.gov

Citation:
Lucco Castello, F., Delzanno, G. L., Borovsky, J. E., Miars, G., Leon, O., & Gilchrist, B. E. (2018). Spacecraft-charging mitigation of a high-power electron beam emitted by a magnetospheric spacecraft: Simple theoretical model for the transient of the spacecraft potential. *Journal of Geophysical Research: Space Physics*, *123*, 6424–6442. https://doi.org/10.1029/2017JA024926

Received 26 OCT 2017
Accepted 14 MAY 2018
Accepted article online 29 MAY 2018
Published online 17 AUG 2018

©2018. American Geophysical Union. All Rights Reserved.

Spacecraft-Charging Mitigation of a High-Power Electron Beam Emitted by a Magnetospheric Spacecraft: Simple Theoretical Model for the Transient of the Spacecraft Potential

F. Lucco Castello[1], G. L. Delzanno[1], J. E. Borovsky[2], G. Miars[3], O. Leon[4], and B. E. Gilchrist[3]

[1]Theoretical Division, Los Alamos National Laboratory, Los Alamos, NM, USA, [2]Space Science Institute, Boulder, CO, USA, [3]Department of Electrical Engineering and Computer Science, University of Michigan, Ann Arbor, MI, USA, [4]Applied Physics Program, University of Michigan, Ann Arbor, MI, USA

Abstract A spacecraft-charging mitigation scheme necessary for the operation of a high-power electron beam in the low-density magnetosphere is analyzed. The scheme is based on a plasma contactor, that is, a high-density charge-neutral plasma emitted prior to and during beam emission and its ability to emit high ion currents without strong space-charge limitations. A simple theoretical model for the transient of the spacecraft potential and contactor expansion during beam emission is presented. The model focuses on the contactor ion dynamics and is valid in the limit when the ion contactor current is equal to the beam current. The model is found in very good agreement with particle-in-cell simulations over a large parametric study that varies the initial expansion time of the contactor, the contactor current, and the ion mass. The model highlights the physics of the spacecraft-charging mitigation scheme, indicating that the most important part of the dynamics is the evolution of the outermost ion front, which is pushed away by the charge accumulated in the system by the beam. The model can be also used to estimate the long-time evolution of the spacecraft potential. For a short contactor expansion (0.3- or 0.6-ms helium plasma or 0.8-ms argon plasma, both with 1-mA current) it yields a peak spacecraft potential of the order of 1–3 kV. This implies that a 1-mA relativistic electron beam would be easily emitted by the spacecraft.

1. Introduction

There is a rich history of active space experiments involving electron beams, which dates back to the seventies. These experiments used nonrelativistic electron beams with energies up to several tens of kilo-electron volts and currents in some cases up to ∼1 A, with the goal of investigating the charging of space vehicles (Myers et al., 1990), basic plasma physics phenomena such as beam-environment interactions (Hallinan et al., 1978; Neubert et al., 1995; Zhulin et al., 1980) and the generation and propagation of very low frequency waves (Huang et al., 1998; Raitt et al., 1995; Reeves et al., 1990), and various aspects of magnetospheric physics (Hendrickson et al., 1975; Lavergnat, 1982; Nemzek et al., 1992; Nemzek & Winckler, 1991; Pellat & Sagdeev, 1980; Prech et al., 1995, 2002; Swanson et al., 1986; Wilhelm et al., 1980; Winckler, 1980). Reviews of the use of electron beams in space can be found in Winckler (1992) and Neubert and Banks (1992).

In any active space experiment with electron beams, the charging of the vehicle requires critical consideration. The beam current must be compensated by a comparable return current from the environment. If not, the vehicle charges to high electrostatic potentials and electrostatically pulls the beam back to the vehicle. Strong charging, particularly if associated with differential charging across surfaces, could also lead to catastrophic damage of the vehicle. These considerations explain why most of the experiments cited above were performed in the ionosphere, where the plasma has high density and could provide enough return current. The only exception is the Spacecraft Charging at High Altitude (SCATHA, also known as P78-2) experiment, which occurred at geosynchronous orbit in the low-density magnetosphere. While SCATHA was successful in operating electron beams at lower currents (less than ∼100 μA; Gussenhoven et al., 1980), one experiment performed with a beam of 6-mA current and 3-keV energy caused the permanent damage of three payloads

and the interruption of telemetry for several seconds (Cohen et al., 1980). For reference, the thermal electron current associated with typical parameters at geosynchronous orbit is a few $\mu A/m^2$.

A renewed interest toward active experiments has arisen in the last few years, as called for in the recent decadal survey for space physics (National Research Council, 2012), driven by scientific and national security applications. In one application, electron beams are used as magnetic-field-line tracers to unambiguously connect physics phenomena occurring in the magnetosphere with their image in the ionosphere (Borovsky et al., 2000; MacDonald et al., 2012), thus establishing causality between the two and answering long-standing scientific questions related to magnetosphere-ionosphere coupling (Borovsky et al., 2000; Delzanno et al., 2016; MacDonald et al., 2012). Another application is radiation belt remediation, whereby man-made waves (created either by an antenna or an electron beam) can precipitate energetic particles via wave-particle interactions and return the radiation belt fluxes to more benign levels (Inan et al., 2003). A radiation belt remediation scheme could in principle operate in the ionosphere or magnetosphere, but the (equatorial) magnetosphere could be preferable since lower changes in pitch angle would be needed to induce particle precipitation. Thus, both applications would require operating high-power electron beams in the low-density magnetosphere.

How can we use high-power electron beams on magnetospheric spacecraft without incurring significant spacecraft charging? First, we note that the recent development of compact, relativistic electron accelerators substantially reduces spacecraft-charging problems. In fact, assuming that one needs 1 kW of power injected into the environment, a 10-keV electron beam would require a current of 0.1 A, while a 1-MeV beam would only need 1 mA. Second, a spacecraft-charging mitigation scheme is necessary. One possibility is to balance the electron beam emission current with simultaneous ion beam emission. Modern ion beams currents often exceed 1 mA despite being strongly space-charge-limited compared to electron beams (as ions are significantly more massive than electrons). However, any minute beam current imbalance still leads to rapid spacecraft charging (either positive or negative). To illustrate this phenomenon, imagine the 6-mA electron beam used on the SCATHA spacecraft was balanced with ion beam emission and their beam currents differed by just 1%. The effective emission current of this scenario would be ± 60 μA and a 1-m radius spacecraft in a negligible ambient plasma would still charge to ± 3 kV in just 6 ms. This precludes ion beam neutralization in practice and demands an alternative form of spacecraft charge control. Another possibility for spacecraft-charging mitigation is to use a plasma contactor, that is, a high-density charge-neutral plasma emitted prior to and during beam emission. Plasma contactors have been used many times before to mitigate spacecraft charging (Comfort et al., 1998; Gilchrist et al., 1990; Katz et al., 1994; Olsen, 1985; Prech et al., 1995), and, for instance, a plasma contactor unit is routinely used on the International Space Station. Plasma contactors, however, have not been demonstrated for electron beam experiments on magnetospheric spacecraft, where spacecraft charging would be much more severe than that created by the space environment alone.

Here we focus on a new type of active space experiment aimed at solving long-standing questions on magnetosphere-ionosphere connectivity (Borovsky et al., 2000; Delzanno et al., 2016; MacDonald et al., 2012). In this scenario, a 1-mA/1-MeV pulsed (0.5 s on, 0.5 s off) electron beam creates a signature in the atmosphere that can be detected optically or with radars during auroral activity (Dors et al., 2017). The spacecraft orbits in the low-density outer magnetosphere, targeting the transition region between dipolar and stretched magnetic field lines. The requirements of successful emission of the electron beam and safe operation of the spacecraft imply that the spacecraft should not charge to more than a few kilovolts. Spacecraft-charging mitigation would be achieved by a standard plasma contactor, which uses a noble gas (typically xenon or argon, but helium could also be used) and can deliver currents up to $\sim$1 A, with electron volt (sub-electron volt) temperatures for electrons (ions) and ion drift velocities of the order of 10 km/s.

For such experiments, Delzanno et al. (2015a, 2015b) recently performed particle-in-cell (PIC) numerical simulations of the early-time interaction between a spacecraft, a plasma contactor, and an electron beam either in vacuum or in the low-density magnetospheric plasma. The main result of this investigation is that the contactor cannot be used to *make contact* with the magnetospheric plasma and increase the electron collection area of the spacecraft, as previously thought. Rather, the contactor could be used to mitigate spacecraft charging by broadly emitting substantial ion currents (without the well-known space-charge limitations that one would instead have for an ion beam). While promising, these PIC simulation results are only applicable to the early-time evolution of a real space experiment, and predictions of the long-time evolution of the system are still critically needed to assess its feasibility.

In this paper we present a simple mathematical model that describes the transient of the spacecraft potential during contactor and electron beam emission for the conditions outlined above. The main results of our investigation are twofold. First, we show that the model reproduces the results of self-consistent PIC simulations with remarkable accuracy and over a large range of parameters, thus highlighting the physics behind the charge-mitigation scheme clearly. Second, it provides a useful tool to quickly estimate the long-time evolution of the system (overcoming the limitations of PIC simulations) and assess the feasibility of a contactor/beam experiment in the low-density magnetosphere. We emphasize that such experiments would operate in a new regime, where available data from past active experiments are of little use for validation or feasibility: beam/contactor experiments have been performed before in the ionosphere, but the background plasma has orders-of-magnitude higher density and is substantially more collisional. Thus, modeling and simulations are necessary to study feasibility of these new type of active experiments before they can be credibly proposed.

The paper is organized as follows. In section 2 we describe our base model for the transient evolution of the spacecraft potential during contactor and beam emission. In section 3 we introduce further simplifications to the base model in order to assess the importance of the various aspects of the model and show the physics behind the charge-mitigation scheme clearly. In section 4, we compare the various models against PIC simulations, showing that, as expected, the base model is indeed the most accurate. The agreement with PIC is very good over a large set of parameters, including studies where we change the beam/contactor currents and the ion mass. Last, we use the base model to investigate the long-time evolution of the spacecraft potential when the outer domain boundary where the electrostatic potential goes to zero is set to infinity. For the parameters considered, the spacecraft potential reaches values of the order of 1 kV, much lower than the beam energy of a relativistic beam. This implies that the beam could easily be emitted by the spacecraft. Conclusions are drawn in section 5.

2. Physics Model of Spacecraft Potential and Contactor Dynamics During Beam Emission

In this section we present the equations for the semianalytical models that we developed to study the transient of the spacecraft potential and contactor plasma dynamics during beam emission (Delzanno et al., 2015a, 2015b). Note that in the following derivation the temperature is normalized as $\hat{T}_s = T_s/T_{\mathrm{ref}}$, the density as $\hat{n}_s = n_s/n_{\mathrm{ref}}$, the length as $\hat{x} = x/\lambda_{\mathrm{ref}}$, the velocity as $\hat{v} = v/v_{\mathrm{th,ref}}$, the time as $\tau = t\omega_{p,\mathrm{ref}}$, the electrostatic potential as $\psi = e\phi/k_B T_{\mathrm{ref}}$, the current as $\hat{I}_s = I_s/en_{\mathrm{ref}}v_{\mathrm{th,ref}}\lambda_{\mathrm{ref}}^2$ and the charge as $\mathcal{Q} = Q/en_{\mathrm{ref}}\lambda_{\mathrm{ref}}^3$, where $\hat{v}_{\mathrm{th,ref}} = \sqrt{k_B T_{\mathrm{ref}}/m_e}$ is a reference thermal velocity, $\lambda_{\mathrm{ref}} = \sqrt{\epsilon_0 k_B T_{\mathrm{ref}}/e^2 n_{\mathrm{ref}}}$ is a reference Debye length, $\omega_{p,\mathrm{ref}} = \sqrt{e^2 n_{\mathrm{ref}}/m_e\epsilon_0}$ is a reference electron plasma frequency, e is the positive elementary charge, k_B is the Boltzmann constant, m_e is the electrons mass, and ϵ_0 is the dielectric constant of vacuum. Subscript s is also introduced to label the plasma species, with $s = e\,(i)$ for electrons (ions). In general, hatted quantities denote normalized variables.

We study the mutual interaction of a system consisting of the spacecraft, the electron beam, and the plasma contactor. Two different regimes are identified in the spacecraft-charging process. For time $\tau < 0$ the spacecraft is only emitting a plasma contactor with ion current $\hat{I}_i$ and electron current $\hat{I}_e$. Note that formally $\hat{I}_e > \hat{I}_i$ but in a short initial transient the spacecraft charges positively to equilibrate the ion and electron contactor currents. We call this regime the *contactor expansion*. For $\tau \geq 0$ we enter in the *beam emission* regime, where an electron beam with current $\hat{I}_b$ is emitted together with the plasma contactor.

2.1. Assumptions

In this subsection we discuss the equations of the model describing the transient of the spacecraft potential once the beam is turned on, while the injection of the contactor plasma is maintained. The model is based on the following assumptions.

A1. The system is spherically symmetric. The spacecraft is modeled as a sphere of radius $\hat{r}_1$ at potential $\psi_{\mathrm{sc}} = \psi(\hat{r}_1) > 0$, while at the outer boundary of the system $\hat{r} = \hat{r}_2$ we assume a grounded wall so that $\psi(\hat{r}_2) = 0$. The electron beam is emitted isotropically from the whole surface of the spacecraft with area $\mathcal{A} = 4\pi\hat{r}_1^2$. The contactor cloud, which controls the spacecraft potential, is identified by two regions: a *quasi-neutral region* that extends from the spacecraft up to position $\hat{r}_{\mathrm{qn}}$ (where the assumption of quasi-neutrality breaks down) and an *ion region* where the ion density, $\hat{n}_i$, is larger than the electron density, $\hat{n}_e$. The ion region extends from the edge of the quasi-neutral cloud, $\hat{r}_{\mathrm{qn}}$, up to the position of the last ion, $\hat{r}_i$, that identifies the ion front

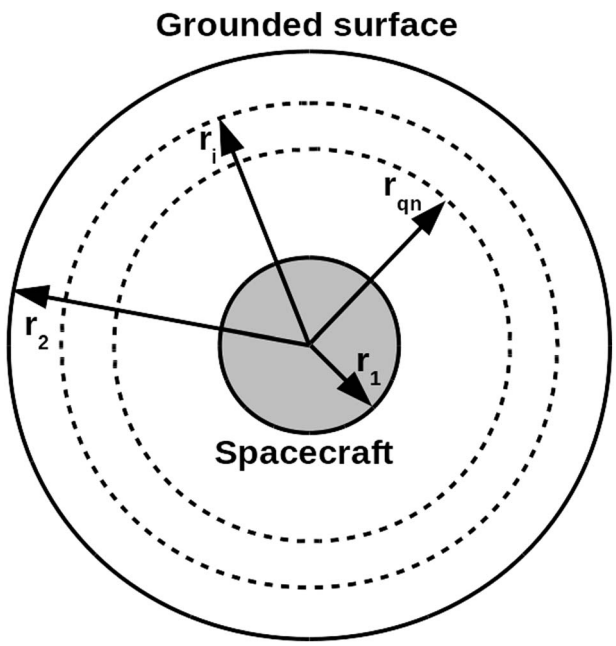

Figure 1. Reference geometry for the theoretical model: r_1 represents the spacecraft radius, r_{qn} is the largest radius where the plasma contactor can be considered quasi-neutral, r_i is the radius of the contactor ion front (i.e., the position of the outermost contactor ion), and r_2 is the radius where the electrostatic potential is set to zero.

and is at potential $\psi_i > 0$. Here the plasma is nonneutral: densities have dropped to very low values, the corresponding Debye length is large, and electrons (if present) and ions do not necessarily move together. The reference geometry is shown in Figure 1. Note that, consistent with the assumption of spherical symmetry, we do not consider an external magnetic field. The magnetic field will affect the geometry of the contactor cloud once the cloud has reached scales comparable to the ion gyroradius and its study is left for the future.

A2. The electron beam has a sufficiently large speed that it can be assumed to leave the system instantaneously, leaving behind a positive charge ($\hat{I}_b\tau$). Note that this assumption is supported by the results presented in Delzanno et al. (2015a) and is well satisfied for a relativistic beam.

A3. The model does not treat electron dynamics in the plasma contactor. Thus, we focus on the case $\hat{I}_b = \hat{I}_i$. This also implies that we do not describe the fast electron-induced transient in the system when the beam is turned on: the electron current from the contactor goes instantaneously from its value $\hat{I}_e$ corresponding to the contactor expansion regime to the value $\hat{I}_e = 0$ of the beam-emission regime and the (quasi-neutral) electron density remains stationary.

A4. The model is electrostatic.

A5. The system evolves on the slow time scale of the ions, in the quasi-static approximation. This means that, at any time, the dynamics is driven by the evolution of the quasi-neutral surface and of the ion front, while the instantaneous electric field configuration is given by the solution of Poisson's equation where the densities are computed in steady state, within the framework of the orbital-motion-limited (OML) kinetic theory.

A6. We assume that the contactor maintains a constant ion current $\hat{I}_i$ for $\psi_{sc} > 0$. Combined with assumption *A3*, this implies that the beam charge $\hat{I}_b\tau$ is transferred instantaneously to the ion region and that the charge enclosed by the quasi-neutral surface (plus the spacecraft) remains constant when the beam is fired. Note that this charge is not necessarily zero, since during the contactor expansion some fast electrons quickly stream out and leave the system. Nevertheless, we assume that the total charge enclosed by the quasi-neutral cloud and the spacecraft (Figure 1) is zero, since this charge is much smaller than the charge that is accumulated in the system during beam emission. This means that the electric field at $\hat{r}_{qn}$ is also zero:

$$\left.\frac{d\psi}{d\hat{r}}\right|_{\hat{r}_{qn}} = 0, \tag{1}$$

as dictated by Gauss' law. Equation (1) provides one boundary condition for Poisson's equation as discussed below.

A7. At injection, contactor ions are cold with finite drift velocity, while electrons are injected according to a Maxwellian at rest since their thermal velocity is much larger than the ion drift velocity. This is consistent with experimental results obtained with hollow cathodes (Bell et al., 2017; Kameyama & Wilbur, 2000).

A8. There is no potential drop across the quasi-neutral region. In principle, one could account for it with a correction proportional to the electron temperature of the plasma contactor. In practice, the electron temperature is much smaller than the values of the transient spacecraft potential and the potential drop across the quasi-neutral region quickly becomes negligible. Thus, the spacecraft potential is equal to the potential at the position of the quasi-neutral cloud, $\psi(\hat{r}_1) = \psi(\hat{r}_{qn})$.

A9. Vacuum is assumed beyond the ion front, $\hat{r} > \hat{r}_i$. This is a conservative assumption, justified from Delzanno et al. (2015b) where we showed that the presence of a low-density background plasma such as that of the outer magnetosphere reduces the spacecraft potential slightly relative to the vacuum case. It is also consistent with assumption *A3*, since for $\hat{I}_b < \hat{I}_i$ contactor electrons would be present for $\hat{r} > \hat{r}_i$ and we would have a region with $\hat{n}_e > 0$ and $\hat{n}_i = 0$.

Finally, the model has four unknowns: the radius of the quasi-neutral cloud, $\hat{r}_{qn}$, the position of the ion front, $\hat{r}_i$, the potential of the ion front, ψ_i, and the spacecraft potential, ψ_{sc}. All these quantities can evolve in time, and we now proceed to describe their equations based on the assumptions listed above.

2.2. Equation for the Position of the Quasi-Neutral Cloud

In general, the dynamics of the quasi-neutral cloud requires modeling of the electron dynamics. This is because when the beam is turned on, the net electron contactor current is reduced to give $\hat{I}_b + \hat{I}_e \simeq \hat{I}_i$ (Delzanno et al., 2015a), and therefore, some (or all) contactor electrons are reabsorbed by the spacecraft. In the limit when $\hat{I}_b = \hat{I}_i$, however, the simulation results of Delzanno et al. (2015a) show that the electron contactor cloud readjusts quickly and then remains constant. Thus, in our model, we use

$$\hat{r}_{qn}(\tau) = \hat{r}_{qn,0}, \tag{2}$$

where $\hat{r}_{qn,0}$ is a constant. Note that, using as guidance the fact that the Child-Langmuir law (Child, 1911) scales with the inverse of the distance between emitter and collector surfaces, it is expected that the influence of equation (2) becomes less important as the ion front expands and $\hat{r}_i \gg \hat{r}_{qn}$.

2.3. Equation for the Position of the Ion Front

The equation for $\hat{r}_i$ is obtained starting from the ion equation of motion

$$\frac{d^2\hat{r}_i}{d\tau^2} = \frac{m_e}{m_i}\mathcal{E}(\hat{r}_i), \tag{3}$$

where $\mathcal{E}(\hat{r}_i)$ is the electric field at $\hat{r}_i$ and m_i/m_e is the ion-to-electron mass ratio. The electric field can be obtained by a simple application of Gauss' law in spherical geometry:

$$\mathcal{E}(\hat{r}_i) = \frac{\mathcal{Q}}{4\pi\hat{r}_i^2}, \tag{4}$$

with $\mathcal{Q}$ representing the total charge inside the sphere of radius $\hat{r}_i$. Since we assume $\hat{I}_b = \hat{I}_i$ (i.e., zero electron current collected at the grounded surface, assumption *A3*), the only current crossing the ion front is the beam current (assumption *A2*) such that

$$\left.\frac{d\mathcal{Q}}{d\tau}\right|_{\hat{r}_i} = \hat{I}_b. \tag{5}$$

See Figure 2. Thus,

$$\mathcal{Q} = \mathcal{Q}_0 + \hat{I}_b\tau, \tag{6}$$

where $\mathcal{Q}_0$ is the charge in the sphere with radius $\hat{r}_i$ at $\tau = 0$.

We substitute equations (4) and (6) into equation (3). This leads to

$$\frac{d^2\hat{r}_i}{d\tau^2} = \frac{m_e}{m_i}\frac{\mathcal{Q}_0 + \hat{I}_b\tau}{4\pi\hat{r}_i^2}. \tag{7}$$

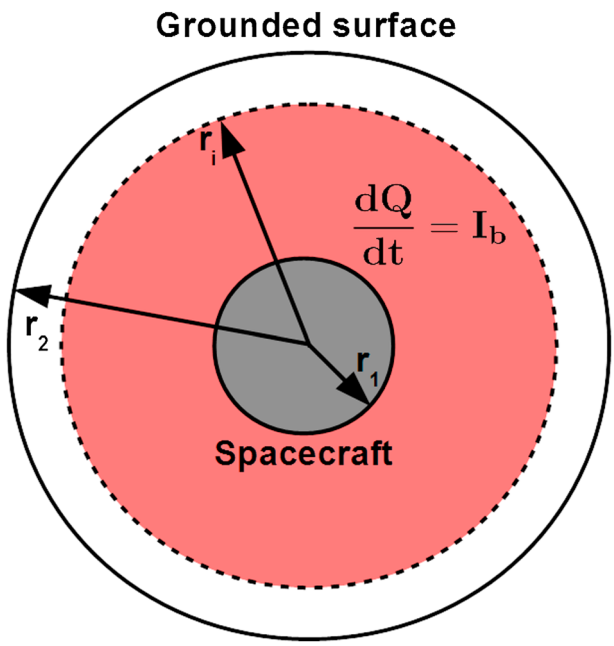

Figure 2. Charge accumulated inside the sphere of radius r_i.

2.4. Equation for the Electrostatic Potential at the Ion Front

We can also compute the electrostatic potential ψ_i at $\hat{r} = \hat{r}_i$. This can be done by solving Poisson's equation in vacuum ($\hat{r} \geq \hat{r}_i$) with boundary conditions given by equation (4) and by $\psi(\hat{r}_2) = 0$ or, equivalently, by introducing a vacuum capacitance

$$C = 4\pi \frac{\hat{r}_2 \hat{r}_i}{\hat{r}_2 - \hat{r}_i} \tag{8}$$

such that

$$\psi_i = \frac{Q}{C} = \frac{Q_0 + \hat{I}_b \tau}{4\pi} \frac{\hat{r}_2 - \hat{r}_i}{\hat{r}_2 \hat{r}_i}. \tag{9}$$

2.5. Equation for the Spacecraft Potential

The equation for the spacecraft potential ψ_{sc} is obtained implicitly from the solution of a nonlinear Poisson equation defined in the ion region, $\hat{r} \in [\hat{r}_{qn}, \hat{r}_i]$:

$$\frac{1}{\hat{r}^2} \frac{d}{d\hat{r}} \left(\hat{r}^2 \frac{d\psi}{d\hat{r}} \right) = \hat{n}_e - \hat{n}_i. \tag{10}$$

Equation (10) is solved including both electron and ion densities, and with boundary conditions given by $d\psi/d\hat{r}|_{\hat{r}=\hat{r}_{qn}} = 0$ (equation (1), assumption *A6*) and $\psi(\hat{r}_i) = \psi_i$ (equation (9), assumption *A9*). Note that the first boundary condition is on the same path followed by Child (1911), when he derived the well-known law for the space-charge-limited current that can flow in a planar diode. In our case, however, the finite ion injection velocity implies that the condition of zero electric field does not identify the maximum current that can flow in the diode, as proven in Jaffe (1944) and later in Akimov et al. (2001).

To solve Poisson's equation, we need to define the densities $\hat{n}_i$ and $\hat{n}_e$ and we use steady state expressions consistent with the currents that are flowing from the quasi-neutral surface into the ion region. For cold ions (i.e., $\hat{T}_i = 0$), we obtain the ion density from a simple application of the ion continuity and momentum equations in steady state:

$$\hat{n}_i = \frac{\hat{I}_b}{4\pi \hat{v}_d \hat{r}^2} \left(1 + \frac{\psi_{sc} - \psi}{\mathcal{K}_i} \right)^{-\frac{1}{2}} \tag{11}$$

where $\hat{v}_d$ is the ion drift velocity, $\mathcal{K}_i = m_i/m_e \hat{v}_d^2/2$ is the ion kinetic energy related to $\hat{v}_d$ and $\psi_{sc} = \psi(\hat{r}_1) = \psi(\hat{r}_{qn})$ is the spacecraft potential. For electrons, we assume a Maxwellian distribution at the quasi-neutral

surface and we apply the kinetic theory derived by Delzanno and Tang (2016) in the OML approximation (see also Tang & Delzanno, 2014):

$$\begin{aligned}\hat{n}_e = &\sqrt{\frac{\pi}{2}}\frac{\hat{J}_e}{\hat{v}_{\mathrm{th},e}}\exp\left(\frac{\psi-\psi_{\mathrm{sc}}}{\hat{T}_e}\right)\\ &\times\left[1+\mathrm{erf}\sqrt{\frac{\psi}{\hat{T}_e}}-\frac{2}{\sqrt{\pi}}\sqrt{\frac{\psi}{\hat{T}_e}}\exp\left(-\frac{\psi}{\hat{T}_e}\right)\right.\\ &\left.-\frac{\sqrt{z^2-1}}{z}\exp\left(\frac{\psi-\psi_{\mathrm{sc}}}{\hat{T}_e(z^2-1)}\right)\right],\\ &\text{if } \psi(z)\le\psi_{\mathrm{sc}}/z^2\end{aligned} \tag{12}$$

$$\begin{aligned}\hat{n}_e = &\sqrt{\frac{\pi}{2}}\frac{\hat{J}_e}{\hat{v}_{\mathrm{th},e}}\exp\left(\frac{\psi-\psi_{\mathrm{sc}}}{\hat{T}_e}\right)\left[1+\mathrm{erf}\sqrt{\frac{\psi}{\hat{T}_e}}\right.\\ &+\frac{2}{\sqrt{\pi}}\left(\sqrt{\frac{1}{\hat{T}_e}\left(\psi-\frac{\psi_{\mathrm{sc}}}{z^2}\right)}-\sqrt{\frac{\psi}{\hat{T}_e}}\right)\\ &\times\exp\left(-\frac{\psi}{\hat{T}_e}\right)-\frac{\sqrt{z^2-1}}{z}\exp\left(\frac{\psi-\psi_{\mathrm{sc}}}{\hat{T}_e(z^2-1)}\right)\\ &\left.\times\left(1+\mathrm{erf}\sqrt{\frac{1}{\hat{T}_e}\frac{z^2\psi-\psi_{\mathrm{sc}}}{z^2-1}}\right)\right],\\ &\text{if } \psi(z)\ge\psi_{\mathrm{sc}}/z^2\end{aligned} \tag{13}$$

where $\hat{J}_e$ is the electron current density at $\hat{r}_{\mathrm{qn}}$, $\hat{T}_e$ is the electron temperature, $\hat{v}_{\mathrm{th},e}$ is the electron thermal velocity and $z=\hat{r}/\hat{r}_{\mathrm{qn}}$. The electron current density $\hat{J}_e$ is obtained by imposing quasi-neutrality at $\hat{r}_{\mathrm{qn}}$; that is, $\hat{n}_e(\hat{r}_{\mathrm{qn}})=\hat{n}_i(\hat{r}_{\mathrm{qn}})$, from which it follows that

$$\hat{J}_e=\frac{\hat{I}_i}{4\pi\hat{r}_{\mathrm{qn}}^2}\frac{\hat{v}_{\mathrm{th},e}}{\hat{v}_d}\sqrt{\frac{2}{\pi}}\times\left[1+\mathrm{erf}\sqrt{\frac{\psi_{\mathrm{sc}}}{\hat{T}_e}}-\frac{2}{\sqrt{\pi}}\sqrt{\frac{\psi_{\mathrm{sc}}}{\hat{T}_e}}\exp\left(\frac{\psi_{\mathrm{sc}}}{\hat{T}_e}\right)\right]^{-1}. \tag{14}$$

Note that the formulation of the densities (12) and (13) supports a finite electron current in the system given by (Delzanno & Tang, 2016)

$$\hat{I}_e=4\pi\hat{r}_1^2\hat{J}_e\left(1+\frac{\psi_{\mathrm{sc}}}{\hat{T}_e}\right)\exp\left(-\frac{\psi_{\mathrm{sc}}}{\hat{T}_e}\right). \tag{15}$$

In practice, however, the transient values of the spacecraft potential are much higher than the electron temperature and the electron current is practically zero. This also justifies why the ion density (equation (11)) is computed with the beam current.

From equations (10)–(14), we can compute the electrostatic potential in $\hat{r}\in[\hat{r}_{\mathrm{qn}},\hat{r}_i]$ and use assumption *A8* to obtain the spacecraft potential $\psi_{\mathrm{sc}}=\psi(\hat{r}_{\mathrm{qn}})$.

In summary, our model to study the evolution of the spacecraft potential in the beam-emission regime consists of equations (2), (7), (9), and (10) with densities given by equations (11)–(14), and boundary conditions given by equation (1) and $\psi(\hat{r}_2)=0$. The spacecraft potential is then $\psi_{\mathrm{sc}}=\psi(\hat{r}_{\mathrm{qn}})$. Note that in this model the dynamics of the ion front is completely decoupled from the rest of the system and depends only on the beam current. We will refer to this model as the *base model*.

3. A Hierarchy of Further Simplified Models to Expose the Physics of Spacecraft-Charging Mitigation via the Plasma Contactor

In this section, starting from the base model described in section 2, we introduce further model simplifications to highlight the various aspects of the model and show clearly the physics of spacecraft-charging mitigation mediated by a plasma contactor.

Table 1
Initial Conditions Required by the Four Models Described in Sections 2 and 3

Model	$\hat{r}_{\mathrm{qn},0}$	$\hat{r}_{i,0}$	$\hat{v}_{i,0}$	$\mathcal{Q}_0$
Base model	×	×	×	×
Model 2		×	×	×
Model 3	×	×	×	×
Model 4	×			

3.1. Model 2, Without Defining the Quasi-Neutral Surface

Model 2 does not use the definition of the quasi-neutral surface, but the rest remains unchanged relative to the base model. This means that $\hat{r}_i$ and ψ_i are still described by equations (7) and (9), while Poisson's equation used to find ψ_{sc} is solved in $\hat{r} \in [\hat{r}_1, \hat{r}_i]$. Solving Poisson's equation from $\hat{r}_1$ requires three modifications. First, the boundary conditions become $\mathrm{d}\psi/\mathrm{d}\hat{r}|_{\hat{r}=\hat{r}_1} = 0$ and $\psi(\hat{r}_i) = \psi_i$. (Note that, relative to the results that are presented below, we have also tried using a boundary condition $\mathrm{d}\psi/\mathrm{d}\hat{r}|_{\hat{r}=\hat{r}_1} = -\mathcal{Q}_{\mathrm{sc}}/(4\pi\hat{r}_1^2)$, where the charge on the spacecraft $\mathcal{Q}_{\mathrm{sc}}$ was taken from PIC simulations but without finding much difference in the results.) Second, the definition of z in equations (12) and (13) is changed to $z = \hat{r}/\hat{r}_1$. Third, equation (14) has to be modified into $\hat{J}_e = \hat{I}_e^{\mathrm{inj}}/\mathcal{A}$, where $\hat{I}_e^{\mathrm{inj}}$ represents the electron current that the contactor injects in the system and that returns to the spacecraft due to space-charge effects, such that $\hat{I}_e = 0$. Model 2 is designed to highlight the role of the quasi-neutral surface.

3.2. Model 3, Without Electrons in the Ion Region

Model 3 does not include electrons in Poisson's equation in the ion region, while everything else remains the same. Thus, Poisson's equation (10) becomes

$$\frac{1}{\hat{r}^2}\frac{\mathrm{d}}{\mathrm{d}\hat{r}}\left(\hat{r}^2\frac{\mathrm{d}\psi}{\mathrm{d}\hat{r}}\right) = -\frac{\hat{I}_b}{4\pi\hat{v}_d\hat{r}^2}\left(1+\frac{\psi_{\mathrm{sc}}-\psi}{\mathcal{K}_i}\right)^{-\frac{1}{2}} \tag{16}$$

and is solved with boundary conditions $\mathrm{d}\psi/\mathrm{d}\hat{r}|_{\hat{r}=\hat{r}_{\mathrm{qn}}} = 0$ and $\psi(\hat{r}_i) = \psi_i$. Model 3 is designed to highlight the role of electrons in the ion region: even though $\hat{I}_b = \hat{I}_i$ and $\hat{I}_e = 0$, the density of (trapped) electrons that are reabsorbed by the spacecraft can play a role in the vicinity of the quasi-neutral surface.

3.3. Model 4, Without Electrons in the Ion Region and Without Defining the Ion Front

Model 4 does not consider the electrons in the ion region (as in model 3) and eliminates the definition of the ion front in the model. This means that $\hat{r}_{\mathrm{qn}}$ is obtained as in the base model, while equations (7) and (9) are not used. The spacecraft potential ψ_{sc} is found from Poisson's equation (16) solved in the domain $\hat{r} \in [\hat{r}_{\mathrm{qn}}, \hat{r}_2]$ with boundary conditions given by $\mathrm{d}\psi/\mathrm{d}\hat{r}|_{\hat{r}=\hat{r}_{\mathrm{qn}}} = 0$ and $\psi(\hat{r}_2) = 0$. This also implies that the ion density is finite all the way to $\hat{r} = \hat{r}_2$ and beyond what would be defined by the position of the ion front. Model 4 is designed to highlight the role of the ion front in the transient of the spacecraft potential.

3.4. Initial Conditions

It is clear that the models described in sections 2 and 3 for the beam-emission regime require initial conditions of the system at $\tau = 0$. If we consider the most complete model (base model), we need the following initial conditions: $\hat{r}_{\mathrm{qn},0}$, $\hat{r}_{i,0}$, $\hat{v}_{i,0}$ and $\mathcal{Q}_0$, where $\hat{v}_i$ is the ion front velocity and its initial condition is needed because the equation of motion for $\hat{r}_i$ is a second-order ordinary differential equation. A subset of these initial conditions is necessary for the reduced models of section 3, as summarized in Table 1.

Obtaining the initial conditions for the equations presented in section 2 would require a model for the contactor expansion that occurs prior to the beam emission. Since in this paper we are interested in highlighting the spacecraft-charging mitigation physics, in the next sections we will take the initial conditions directly from the PIC simulations. The development of a contactor expansion model without beam emission will be deferred to a future publication.

4. Results

4.1. Comparison Between the Semianalytic Models and PIC Simulations

In this section we compare the semianalytic models presented in sections 2 and 3 to PIC simulations performed with the curvilinear particle-in-cell (CPIC) code. The description of CPIC can be found in Delzanno et al.

(2013) and Meierbachtol et al. (2017). Regarding the semianalytic models, the equation for the ion front (7) is solved with an ordinary differential equation solver based on an explicit Runge-Kutta method, while Poisson's equation is solved with the Jacobian-Free Newton-Krylov technique presented in Kelley (1995).

An important point in the PIC simulations concerns the injection of the plasma contactor. As discussed in assumption *A7*, electrons and ions are injected from Maxwellian distribution functions, which require density, temperature, and drift velocity as input. Here we fix the contactor electron and ion temperature, the ion drift velocity, and the ion current, from which the ion density can be easily computed. We inject the contactor electrons and ions with *equal densities*, as done in Delzanno et al. (2015a, 2015b). This means that at injection the electron contactor current is higher than the ion contactor current and that a presheath-like potential drop is established in the quasi-neutral region to equilibrate them. Another possibility would have been to inject the contactor electron and ions with *equal currents*. In this case the electron and ion densities at injection would not be equal due to the different injection velocities, a sheath would arise, and the contactor currents would be reduced to an unknown value that depends on the space-charge electric field created in the system. Furthermore, we have also performed simulations of the contactor expansion and beam-emission phases with equal-current injection (not shown). Relative to the results with equal-density injection presented below, the spacecraft potential shows a similar trend but with generally higher values (for simulation B_1 with helium it peaks at $\psi_{sc} \sim 160$). However, the system loses the quasi-neutral region during beam emission. Since the latter is consistently measured in our ongoing experiments to validate the spacecraft-charging mitigation scheme based on the plasma contactor (Miars et al., 2017), it provides further evidence that equal-density injection is the appropriate injection scheme to treat the plasma contactor: It allows us to seed the quasi-neutral region while specifying (i.e., controlling) the ion contactor current in the system.

4.1.1. Input Parameters

Both the models and CPIC use the normalized variables presented at the beginning of section 2. The normalized parameters used for the comparison are relevant to a magnetosphere-ionosphere-connectivity experiment in the outer magnetosphere (Dors et al., 2017) and are as follows:

1. Geometrical parameters: $\hat{r}_1 = 8.9$, $\hat{r}_2 = 890$, and $\mathcal{A} = 995$.
2. Plasma parameters: $\hat{T}_e = 1$, $\hat{T}_i = 0.2$, $\hat{I}_i = 77.6$, $\hat{I}_e^{\text{inj}} = 560$, $\hat{v}_d = 0.055$, and $m_i/m_e = 7,344$.
3. Beam parameters: $\hat{I}_b = 77.6$.

We consider two cases characterized by a different contactor expansion time prior to beam emission, τ_c. Simulation B1 has $\tau_c = 1,500$ and simulation B2 has $\tau_c = 3,000$. The beam emission time, τ_b, is 10,000 for both B1 and B2. Note that, while the base model and models 3 and 4 use the notion of quasi-neutral surface and fix $\hat{I}_e = 0$, in the PIC simulations a finite electron contactor current is injected in the system, $\hat{I}_e^{\text{inj}}$, and its full transient in response to the dynamics of the system is captured self-consistently.

If we assume $T_{\text{ref}} = 2.3$ eV and $n_{\text{ref}} = 10^4 \text{cm}^{-3}$, the normalized parameters presented above give a domain that extends from $r_1 = 1$ m to $r_2 = 100$ m and a helium plasma contactor emitted with temperatures $T_e = 2.3$ eV and $T_i = 0.5$ eV and with a drift velocity of 35 km/s. For the same reference parameters, the emitted currents are $I_i = I_b = 1$ mA and $I_e^{\text{inj}} = 7.2$ mA, the contactor expansion time before beam emission is $t_c = 0.3$ ms for B1 and $t_c = 0.6$ ms for B2, and the beam emission time is $t_b = 1.8$ ms.

As discussed in section 3.4, the semianalytic models require a set of initial conditions to be used. For reference, the initial conditions used in simulations B1 and B2 are summarized in Table 2.

4.1.2. Case With $I_b = I_i = 1$ mA

We compare the results of the base model of section 2 and the reduced models of section 3 with the solution obtained from CPIC. The results for the parameters listed in section 4.1.1 are shown in Figure 3.

From the CPIC simulations one can see that after the beam is fired, the spacecraft potential rises monotonically until an equilibrium is reached. This happens when the ions have reached the outer wall $\hat{r}_2$: At this point the charge that enters the system, $\hat{I}_b\tau$, is equal to the one that leaves the system, $\hat{I}_i\tau$, and, considering also that the quasi-neutral surface is static, the system is in steady state. Comparing simulations B1 and B2, one can see that the asymptotic spacecraft potential is lower for simulation B2 corresponding to a larger initial area of the contactor, confirming what was already found in Delzanno et al. (2015a).

Table 2
Initial Conditions Used in the Base Model and Maximum of the Spacecraft Potential as Obtained Both From the Model, ψ_{sc}^{max}, and From CPIC, $\psi_{sc,CPIC}^{max}$

Simulation	τ_c	$\hat{r}_{qn,0}$	$\hat{r}_{i,0}$	$\hat{v}_{i,0}$	$\mathcal{Q}_0$	ψ_{sc}^{max} $\hat{r}_2 = 890$ $\tau_b = 10^4$	$\psi_{sc,CPIC}^{max}$ $\hat{r}_2 = 890$ $\tau_b = 10^4$	ψ_{sc}^{max} $\hat{r}_2 \longrightarrow \infty$ $\tau_b = 2.5 \cdot 10^6$
A1, helium	1,650	28	152	0.09	3,700	15.7	16.4	57
B1, helium	1,500	77	151	0.10	8,000	88	90	316
C1, helium	1,400	84	157	0.11	10,000	307	301	985
B2, helium	3,000	138	300	0.10	14,000	60	61	300
A1, argon	4,650	52	154	0.03	6,700	34.5	35.2	118
B1, argon	4,200	85	155	0.04	11,000	206	208	657
C1, argon	4,000	86	157	0.04	14,000	701	707	2,050

Note. The beam emission time $\tau_b = 10^4$ is sufficiently large for the ion front to reach $\hat{r}_2 = 890$. The last column shows the application of the base model to realistic parameters of a magnetospheric active experiment where a 1-MeV beam is fired for 0.5 s ($\tau_b = 2.5 \cdot 10^6$).

Generally speaking, the trends of simulations B1 and B2 shown in Figure 3 are similar. Model 2 (magenta curve), where Poisson's equation is solved in $\hat{r} \in [\hat{r}_1, \hat{r}_i]$ and the quasi-neutral surface is not defined, is off by a factor of 2–3 on the asymptotic value of the spacecraft potential. Although the dynamics resembles that of the PIC simulations, model 2 curves are shifted to much larger values of the spacecraft potential. This happens already at $\tau = 0$, where the solution of Poisson's equation is already very far from the initial condition of the PIC simulations: Model 2 creates an initial condition where essentially there are no electrons in the system and there is no quasi-neutral region (not shown). Model 3 (cyan), which does not include the electrons in the ion region, does a good job in reproducing both the initial transient and the asymptotic value of the CPIC simulations. On the latter, the relative error is only about 10% for simulation B1 and 25% for B2. The spacecraft potential, however, is consistently shifted toward higher potentials if compared to the solution given by CPIC. Model 4 (green) does not include electrons in the ion region and does not define the ion front. As expected, it matches the result of model 3 once the ions have reach the outer wall, since at this point $\hat{r}_i = \hat{r}_2$ and the two models are the same. Since the quasi-neutral surface is static and $\hat{r}_i = \hat{r}_2$, model 4 is a static model and cannot capture the initial transient of the system. This indicates the importance of the ion front for an accurate description of the spacecraft potential transient.

From Figure 3, we can deduce that the base model is the most accurate of all models considered in reproducing both the initial transient as well as the asymptotic value of the system. For both simulations B1 and B2, the error on the asymptotic spacecraft potential relative to CPIC is only 2%. Note also that while model 3 is generally in good agreement with CPIC, it is not as accurate as the base model. This indicates that including the electrons and their effect on the space-charge electric field in the ion region, although not critical, leads to better accuracy.

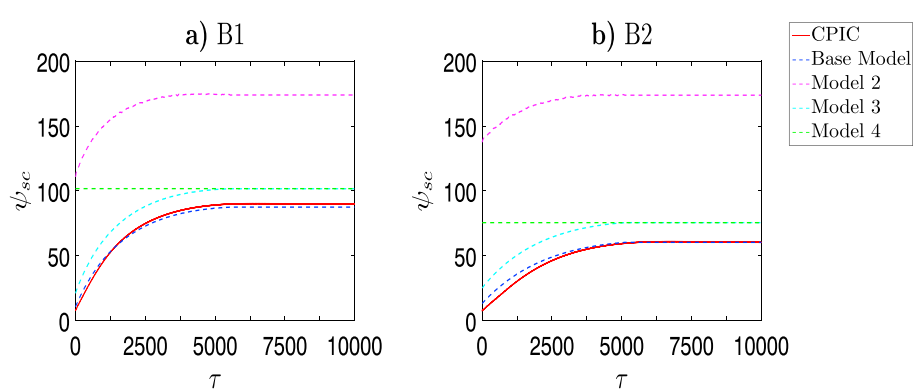

Figure 3. Transient of the spacecraft potential: the base model and models 2–4 (dashed lines) are compared to CPIC (red solid line) for simulations B1 and B2 with helium. CPIC = curvilinear particle-in-cell.

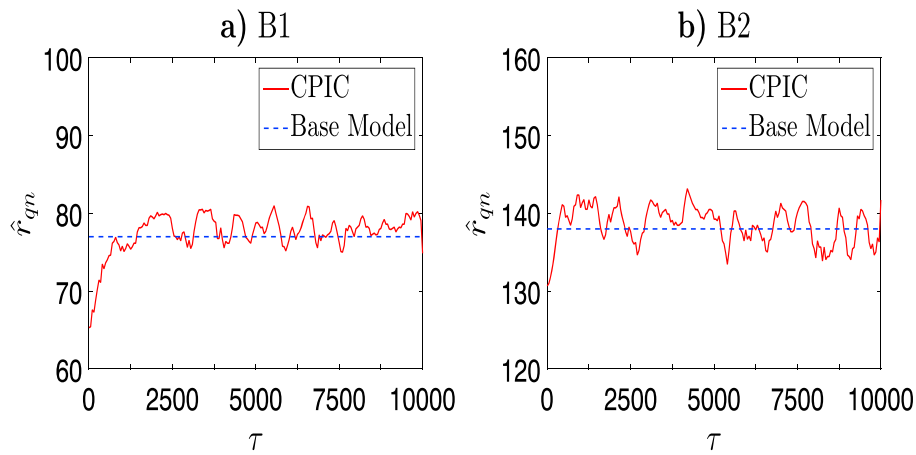

Figure 4. Evolution in time of quasi-neutral cloud position, $\hat{r}_{qn}$, for simulations B1 and B2 with helium: The value used in the base model (blue dashed line) is compared to what was obtained from CPIC (red solid line). CPIC = curvilinear particle-in-cell.

Some remarks can be made from the results presented in this section. First, they show clearly the role of the quasi-neutral surface and of the ion front in determining the transient of the system. It is remarkable that, for the parameters considered, the time evolution of these two surfaces is the most important ingredient of the dynamics of the spacecraft potential and that the dynamics of the ion front depends only on the beam current. Given a set of initial conditions, the ion front can be easily computed by solving equation (7). Then the spacecraft potential can be computed to a good degree of accuracy by solving Poisson's equation (10) only once. Second, considering that the peak of the spacecraft potential is the critical quantity from a mission-design point of view and that for space applications $\hat{r}_2 \longrightarrow \infty$, model 3 (where electrons are essentially neglected apart from their role in defining the quasi-neutral surface) can be considered as the minimal model of contactor and beam emission that compromises between model simplicity and accuracy.

Figures 4–7 show a more in-depth analysis of results of the base model. In particular, Figure 4 shows the value of $\hat{r}_{qn}$ obtained from the CPIC simulations. In order to avoid too much fluctuation induced by statistical noise characteristic of PIC methods, here $\hat{r}_{qn}$ is calculated as the outermost point in the domain where $(n_i - n_e)/n_e < 0.15$, that is, it assumes that quasi-neutrality is broken when the relative density change is at least 15%. We have tried other values of $(n_i - n_e)/n_e$, and, although some cases make the comparison with PIC worse, the general agreement with PIC simulations remains very good. Although statistical noise is visible in Figure 4, the

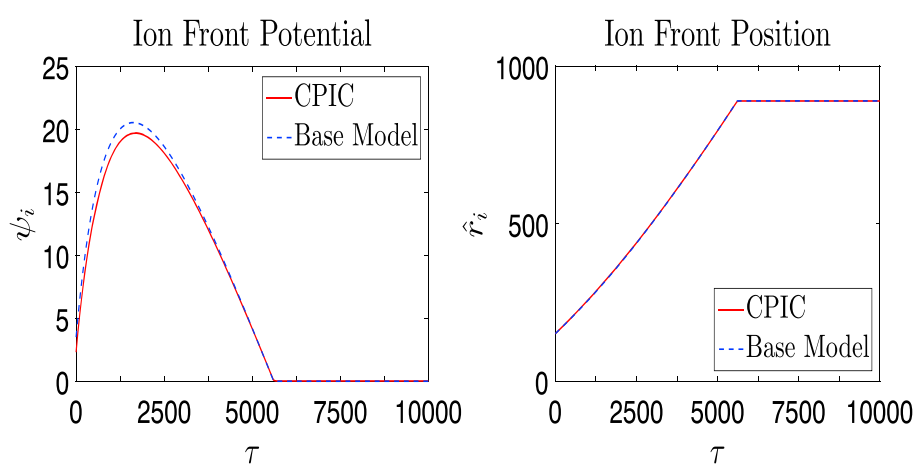

Figure 5. Transient behavior of the position of the ion front, $\hat{r}_i$, and of its potential ψ_i for simulation B1 with helium: The solution obtained with the base model (blue dashed line) is compared to the result given by CPIC (red solid line). CPIC = curvilinear particle-in-cell.

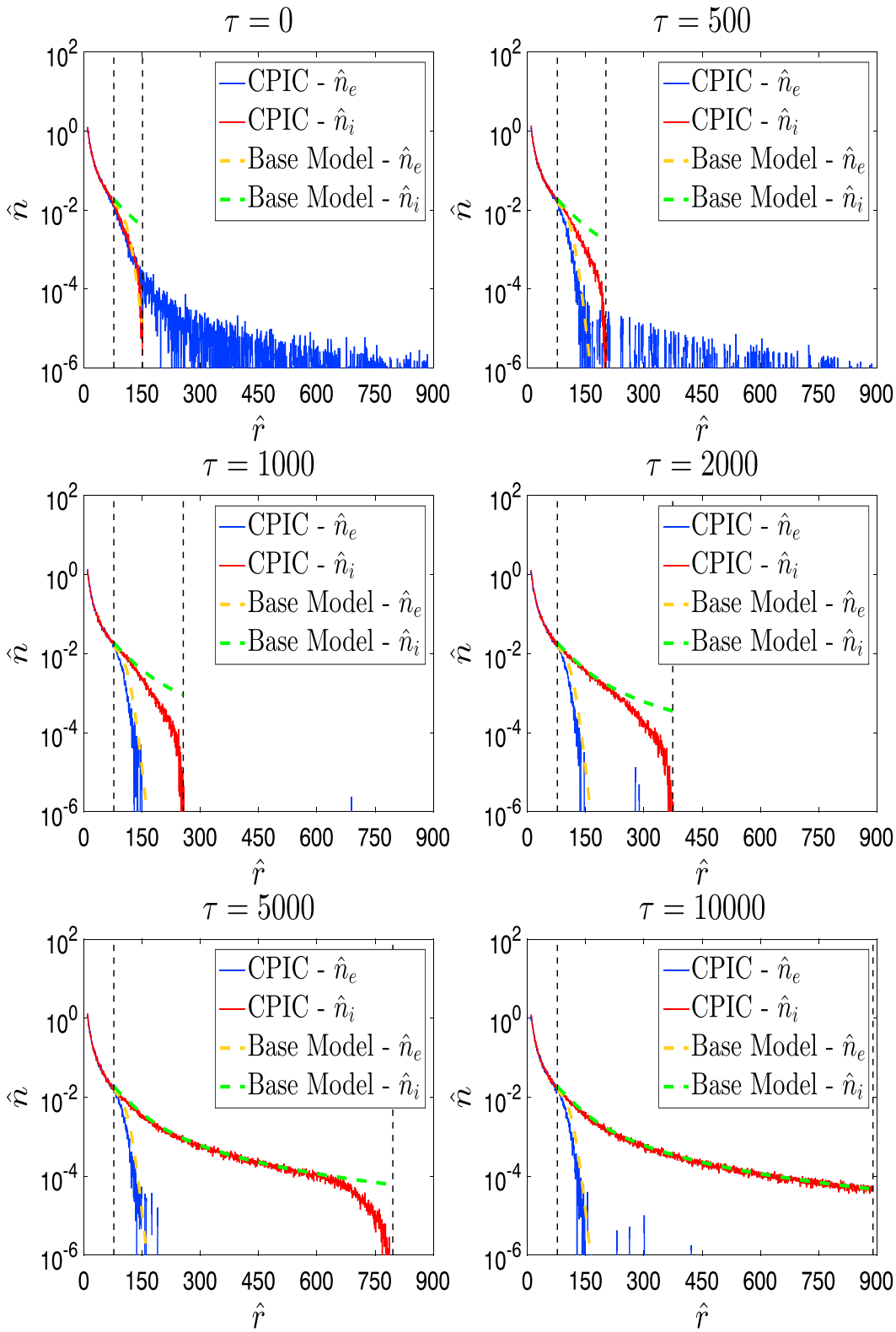

Figure 6. Snapshots of the density profiles for simulation B1 with helium. The CPIC solution (red for the ions and blue for the electrons) is compared to the base model (green for the ions and yellow for the electrons). The black dashed lines represent the position of the quasi-neutral cloud and of the ion front as obtained from the simulations. CPIC = curvilinear particle-in-cell.

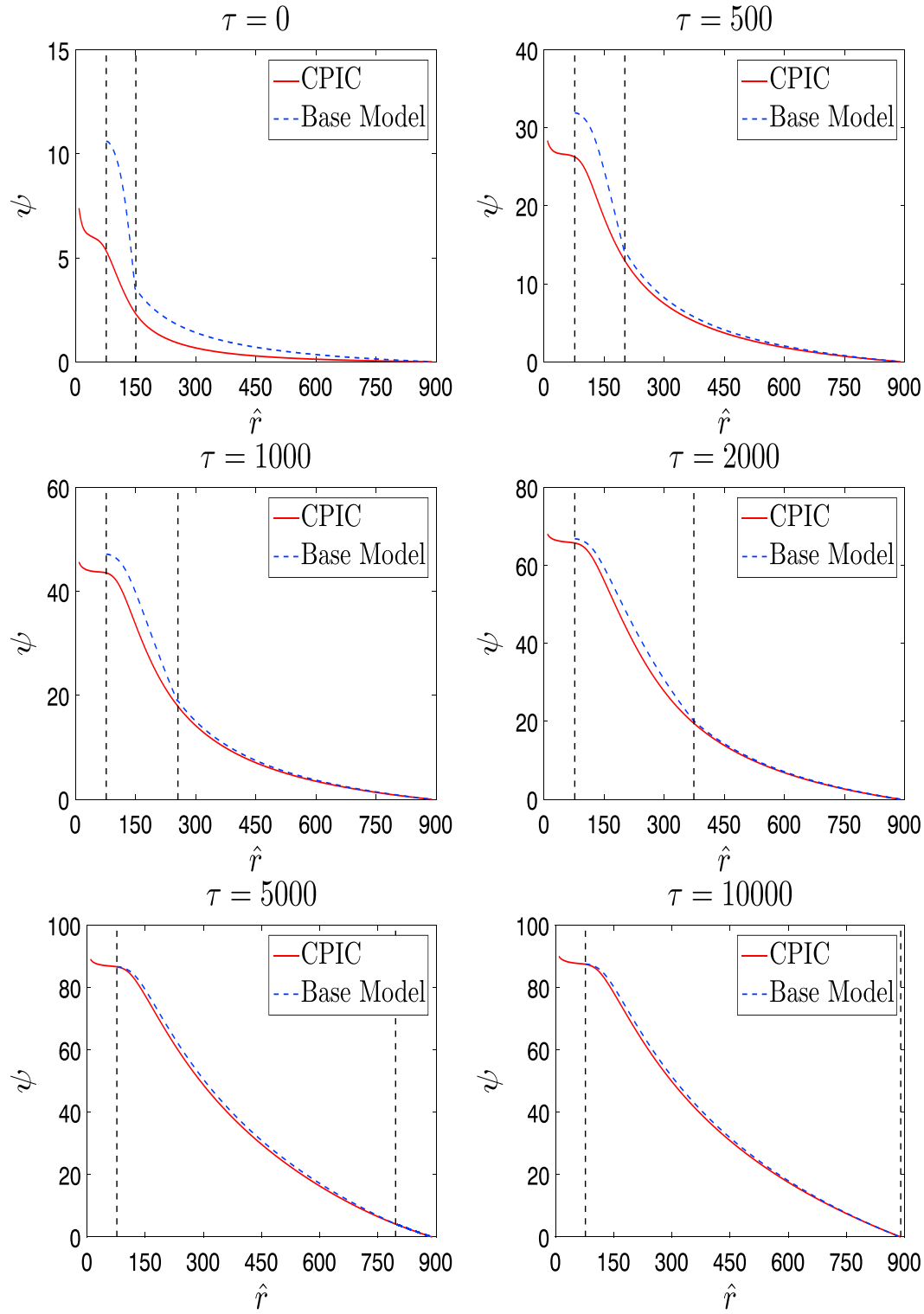

Figure 7. Snapshot of the potential profiles for simulation B1 with helium. The CPIC solution (red solid) is compared to the base model (blue dashed). The black dashed lines represent the position of the quasi-neutral cloud and of the ion front as obtained from the simulations. CPIC = curvilinear particle-in-cell.

plot indicates that a constant $\hat{r}_{qn}$ (equation (2)), as assumed in the semianalytical models, is indeed appropriate and justifies the fact that we have set $\hat{r}_{qn} = 77$ for B1 and $\hat{r}_{qn} = 138$ for B2 for the results of Figure 3.

In Figure 5 we present the transient of $\hat{r}_i$ and ψ_i as obtained from the base model and from CPIC for simulation B1. $\hat{r}_i$ is obtained by the position of the outermost ion in the simulation domain. These plots prove that equations (7) and (9) give an accurate description of the ion front.

Figures 6 and 7 display some snapshots of the density and potential profiles for simulation B1. Let us focus initially on the plots for $\tau = 0$. During the contactor expansion prior to beam emission, some electrons outrun the ions and are in fact responsible for the nonzero electron density beyond the ion front, $\hat{r} > \hat{r}_i$. This leads to a higher potential at the ion front in the base model, as shown in Figure 7 where the vacuum solution (top left panel, dashed line) and the CPIC solution (solid line) can be compared for $\hat{r} > \hat{r}_i$. As the beam is fired and the spacecraft potential grows, electrons are reabsorbed by the spacecraft or leave the system and the vacuum approximation becomes valid. This initial transient occurs on the time scale of the electrons and is therefore very fast: within $\tau \sim 700$ the vacuum approximation is valid and the electron density becomes stationary, consistent with the fact that the net electron current in the system is zero. From Figure 6 we see that the electron density drops quickly to zero at $\hat{r} \sim 150$. The ion density, on the other hand, continues to expand during beam emission until the ions reach the outer wall at $\tau = 5,800$. Then the ion density also becomes stationary.

In terms of the comparison between model and CPIC densities, the biggest discrepancies are at $\tau = 0$ where significant differences are evident. This is not surprising, since our model does not treat the contactor expansion and the initial electron transient in the system. (Also, our definition of where quasi-neutrality breaks and hence the position of the quasi-neutrality surface has much more influence on the solution at the beginning of the transient.) After this transient is exhausted, $\tau > 700$, the agreement between model and CPIC simulations becomes much better. The ion densities are very close to one another except for a small range of radii near the ion front, where the model density goes to zero with a jump, while the CPIC simulation does it smoothly. This is due to the fact the model assumes cold ions, while in the CPIC simulations ions have a finite temperature $\hat{T}_i/\hat{T}_e = 0.2$. Simulations have indeed demonstrated that the discrepancy between the model and CPIC around the ion front is reduced when the ion temperature is further decreased in the CPIC runs (not shown). Once the ions have reached the outer wall, the model and CPIC densities are in excellent agreement. The agreement on the electron density is also good, with the model reproducing the same trend of the simulations and the density dropping quickly to zero at about the same position as in the CPIC results. The comparison between model and simulations on the electrostatic potential (Figure 7) yields similar conclusions: The biggest discrepancies are at $\tau = 0$ but as the transient develops the agreement becomes much better. In Figure 7 one can also see the potential drop in the quasi-neutral cloud, which is of the same order of the electron temperature, obtained from the CPIC simulations. This drop is more relevant in the early phase of the transient, where it represents 20% of the total potential difference between the spacecraft and the outer wall, but it becomes negligible when the spacecraft potential increases. In fact, at $\tau = 5,000$ it is only 2% of the total potential difference.

4.2. Parametric Study

In this subsection we perform a parametric study changing the contactor ion/beam currents, the ion mass, and the domain size. The purpose of this parametric study is twofold: We want to further test the base model with parameters that are different from the ones used in section 4.1, and we are also interested in using the model to possibly identify some scaling laws.

4.2.1. Effect of Varying the Contactor Current

Here we present the results of two more sets of CPIC simulations where we change the contactor current, keeping $\hat{I}_b = \hat{I}_i$. The electron current is changed to maintain $\hat{n}_e = \hat{n}_i$ at injection. We also change the contactor expansion time prior to beam emission, τ_c, to maintain the initial area of the contactor (which affects the transient of the spacecraft potential) approximately constant, as shown in Table 2. All the other parameters remain unchanged from the ones presented in section 4.1 for simulation B1.

We test a case with $\hat{I}_i = \hat{I}_b = 7.8$ and $\hat{I}_e^{inj} = 56$ and a second case with $\hat{I}_i = \hat{I}_b = 388$ and $\hat{I}_e^{inj} = 2,800$. We shall refer to the former case as A1 and to the latter case as C1. Note that, if we assume again $T_{ref} = 2.3$ eV and $n_{ref} = 10^4$ cm^{-3}, simulation A1 corresponds to a contactor current of 0.1 mA and simulation C1 to a contactor current of 5 mA.

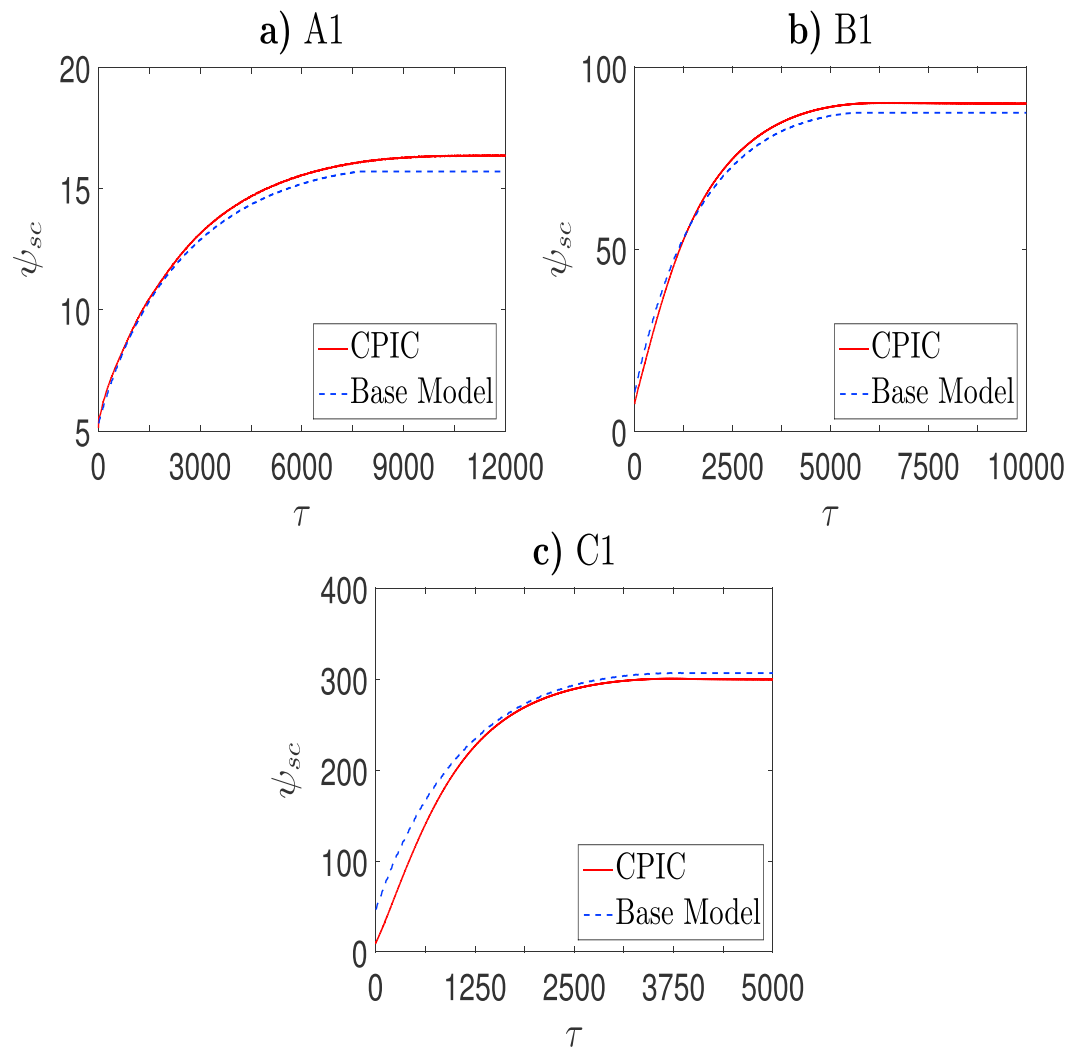

Figure 8. Transient of the spacecraft potential for simulations A1, B1, and C1 with helium. CPIC (red solid) is compared to the base model (blue dashed). CPIC = curvilinear particle-in-cell.

Figure 8 shows the time evolution of the spacecraft potential for simulations A1, B1, and C1. Even with a different contactor current, the base model still gives a good approximation of the system dynamics obtained with CPIC. Owing to the larger spacecraft potential, the asymptotic solution obtained with higher current (C1) is slightly more accurate than the ones obtained with lower currents (the relative errors on the asymptotic spacecraft potential are 4.3%, 2.2%, and 2.0% for A1, B1, and C1, respectively). However, one can also notice that with higher current (C1) the initial transient is not as accurate.

As one would expect, increasing the current leads to a higher spacecraft potential and, thus, to a shorter transient if the value of $\hat{r}_2$ is unchanged. For example, in simulation A1 the ions reach the wall at $\tau = 8,100$, in B1 at $\tau = 5,800$, and in C1 at $\tau = 3,900$. Since all the cases have $\hat{I}_b = \hat{I}_i$, the maximum of the spacecraft potential, ψ_{sc}^{max}, is reached when the ions arrive at the grounded surface. If we focus on the results obtained from the model, we get $\psi_{sc}^{max} = 15.7$ for simulation A1, $\psi_{sc}^{max} = 88$ for simulation B1 and $\psi_{sc}^{max} = 307$ for simulation C1. Considering that $\hat{I}_b^{A1}/\hat{I}_b^{B1} = 10$ and that $\hat{I}_b^{B1}/\hat{I}_b^{C1} = 5$, we obtain

$$\psi_{sc}^{max} \propto \hat{I}_b^{0.76}. \tag{17}$$

Note that this scaling law is different from the one given by Delzanno et al. (2015a), where the authors obtained $\psi_{sc}^{max} \propto \hat{I}_b^{1.2}$. This difference is attributed to the fact that we consider $\hat{I}_b = \hat{I}_i$, while in Delzanno et al. (2015a) the beam current was varied but the contactor current was kept constant.

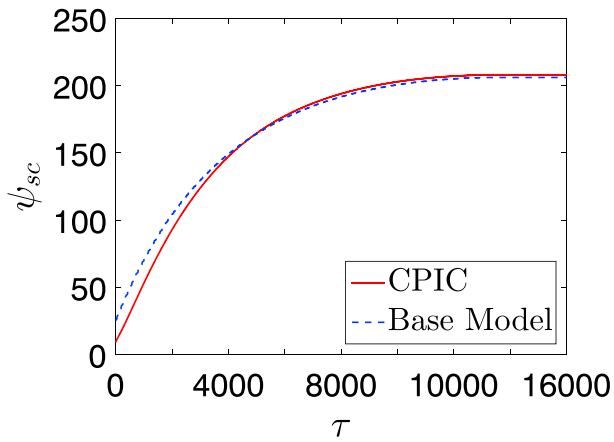

Figure 9. Transient of the spacecraft potential for simulation B1 with argon. CPIC (red solid) is compared to the base model (blue dashed). CPIC = curvilinear particle-in-cell.

4.2.2. Effect of Varying the Ion Mass

We have also performed some simulations with argon, which has an ion mass 10 times higher than helium, $m_i/m_e = 73,400$, in order to compare against the scaling law obtained in Delzanno et al. (2015a).

For argon, we adopt the same currents that were used in simulations A1, B1, and C1 but change the mass ratio, the drift velocity, and the contactor and beam emission times. A different drift velocity is required because if we assume that the argon plasma is produced with the same kinetic energy of the helium plasma, its motion is slower due to the higher mass. Thus, in simulations A1, B1, and C1 with argon we reduce the drift velocity from $\hat{v}_d = 0.055$ to $\hat{v}_d = 0.02$. Moreover, in order to make a comparison between the cases with helium and argon, the initial size of the contactor cloud must be approximately the same, and we need to increase the contactor expansion time τ_c for the argon simulations as shown in Table 2.

Figure 9 shows a comparison between the base model and CPIC for simulation B1 done with argon. The agreement between the two is excellent even for different drift velocity and ion mass, with a 1% error on the asymptotic value of the spacecraft potential. If we compare these results with the one showed in Figure 8b, we see that both CPIC and the model predict a slower transient that leads to a higher spacecraft potential in the case with argon. For simulation B1 with argon the ions require $\tau = 13,800$ to reach $\hat{r}_2$ and at that point the potential is $\psi_{sc}^{max} = 206$.

Table 2 summarizes the values of ψ_{sc}^{max} as obtained from the model for simulations A1, B1, and C1 with helium and argon. All results are in good agreement with CPIC.

From the data in Table 2 we obtain

$$\psi_{sc}^{max} \propto \hat{I}_b^{0.77} \tag{18}$$

for argon. When compared against scaling law (17) for helium, expression (18) indicates that the scaling law of the maximum of the spacecraft potential versus the beam/contactor current does not depend on the ion mass. Furthermore, from Table 2 we obtain

$$\psi_{sc}^{max} \propto \left(\frac{m_i}{m_e}\right)^{\gamma} \tag{19}$$

with $\gamma \in [0.34, 0.37]$. Although expression (19) is only based on three sets of two data points, it is consistent with the scaling law proposed in Delzanno et al. (2015a), $\psi_{sc}^{max} \propto \left(m_i/m_e\right)^{0.4}$.

4.2.3. Effect of the Domain Outer Radius

In all our results so far, we have always assumed the presence of a grounded surface at a finite distance from the spacecraft. This is useful for a model comparison against simulation results, where the computational domain is necessarily finite, and is also relevant to laboratory experiments. However, we can use the base model to explore conditions that are more relevant to a space experiment, where the potential is set to zero at infinity. This can be rather easily imposed in the model, where $\hat{r}_2 \to \infty$ simply leads to changing equation (9) into

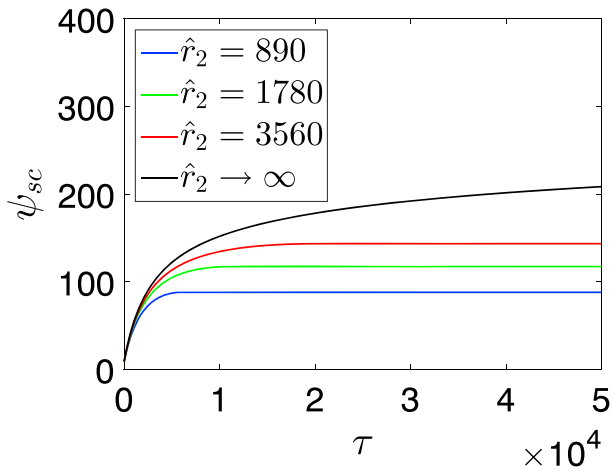

Figure 10. Transient of the spacecraft potential given by the base model for simulation B1 with helium and with different values of the outer radius $\hat{r}_2$.

$$\psi_i = \frac{\mathcal{Q}_0 + \hat{I}_b \tau}{4\pi \hat{r}_i}. \tag{20}$$

All the other equations remain unchanged since they do not depend on $\hat{r}_2$.

In Figure 10, we plot the results obtained from the base model for simulation B1 with helium, varying the outer radius $\hat{r}_2$ of the simulation domain. Increasing the size of the domain has two predictable effects on the spacecraft potential: First, the transient becomes longer and, second, the maximum of the spacecraft potential increases. For instance, the curve obtained with $\hat{r}_2 = 890$ gives $\psi_{sc}^{max} = 88$ and saturates at $\tau = 5,800$, while the curve obtained with a domain four times larger ($\hat{r}_2 = 3,560$), gives $\psi_{sc}^{max} = 145$ and reaches equilibrium only at $\tau = 20,000$. Nevertheless, the most interesting result in Figure 10 is the curve that represents the case with zero potential at infinity. This curve does not saturate (i.e., the system does not reach steady state), as expected since the ions never reach a finite wall while the beam emission continues. The peak of the spacecraft potential will then be reached at a time of the order of the beam emission time.

We have applied the base model to the case of active experiments in the magnetosphere with a relativistic 1-MeV beam fired for 0.5 s (i.e., $\tau = 2.5 \cdot 10^6$). In this case, $\hat{r}_2 \longrightarrow \infty$. The results are presented in Table 2 for all the simulations discussed so far, both with helium and argon. They lead to $\psi_{sc}^{max} \propto \hat{I}_b^{0.73}$ and $\psi_{sc}^{max} \propto \left(\frac{m_i}{m_e}\right)^{0.32}$, in good agreement with the scaling laws discussed above for the case with finite outer domain, $\hat{r}_2 = 890$. For 1-mA current and a short helium contactor expansion of 0.3 ms, the ion front will expand to $\hat{r}_i = 6.7 \cdot 10^5$ (i.e., 75 km) and the spacecraft will charge to $\psi_{sc} \simeq 316$ during the beam firing. This corresponds to approximately 730 V. A helium contactor expansion of 0.6 ms leads to a slightly lower potential of 690 V, while an argon contactor expansion of 0.8 ms leads to 1.5 kV. A 5-mA current with helium (argon) contactor expansion of 0.3 (0.8) ms leads to 2.3 (4.7) kV. All these values are much smaller than the beam energy. Of course, in a realistic situation the contactor is emitted from a narrow injection area, spherical symmetry does not apply, and the spacecraft potential would charge to a higher level than that predicted by our base model. However, the simulation results presented by Delzanno et al. (2015a, 2015b) indicate that the contactor expands quasi-spherically and occupies a fairly large volume of the domain (roughly half) even when injected from a narrow area. This suggests that the spacecraft potential obtained from the spherical model should be multiplied by a factor of order unity for a more realistic prediction. Even in such cases, the spacecraft potential would still be much smaller than the beam energy, implying that the beam would be emitted by the spacecraft. Furthermore, all these arguments apply to a beam-contactor system in a vacuum, while in reality magnetospheric electrons and ions will react to lower the spacecraft potential.

5. Conclusions

In this paper, we have studied a spacecraft-charging mitigation scheme for high-power electron beam active experiments on magnetospheric spacecraft. The scheme is based on a plasma contactor, that is, a high-density neutral plasma emitted prior to and during the electron beam emission. Based on the results of Delzanno

et al. (2015a, 2015b), the contactor mitigates spacecraft charging by emitting a significant ion current off its quasi-neutral surface, well above the ion currents that could be emitted by an ion beam due to space-charge limits.

We have presented a simple mathematical model for the transient of the spacecraft potential and the contactor expansion during beam emission. The model assumes spherical symmetry. It does not treat electron dynamics and is therefore valid when the contactor ion current is equal to the electron beam current, that is, when the net electron-contactor current leaving the system is zero. Furthermore, the contactor dynamics is described by two surfaces: the quasi-neutral surface (which is static for $\hat{I}_b = \hat{I}_i$) and the ion front (which evolves only in response to the beam current). The two surfaces are coupled by Poisson's equation with plasma densities given by the steady state kinetic theory in the OML approximation.

The base model has been compared against self-consistent PIC simulations. It has also been compared against further simplified models with the goal of understanding the importance of the various aspects of the model. Our results demonstrate very good agreement between the base model and PIC over a large parametric study changing the initial contactor cloud area, the beam/contactor current, and the ion mass. It shows the physics of the spacecraft-charging mitigation scheme clearly, highlighting the role of the quasi-neutral and ion front surfaces. It also shows, rather remarkably, that for the parameters considered the most important aspect of the dynamics is the evolution of the ion front, which is controlled only by the beam current. The scaling law of the spacecraft potential versus contactor/beam current was also presented, while results comparing the peak of the spacecraft potential for helium and argon ions are consistent with the scaling law with ion mass found in Delzanno et al. (2015a). One important aspect of the model is its ability to predict the long-time evolution of the system, imposing the zero-potential boundary condition at infinity. Note that this is extremely hard for PIC simulations because of the large spatial- and temporal-scale separation that would need to be bridged.

We have applied the model to support the feasibility of a new type of active space experiment where a relativistic electron beam is used to trace magnetic field lines from magnetosphere to ionosphere (Borovsky et al., 2000). For realistic beam (1-mA current, 1-MeV energy, pulsed every 0.5 s) and plasma contactor (helium plasma with 1-mA current, $T_e = 2.3$ eV, $T_i = 0.5$ eV, ion drift velocity $v_d = 35$ km/s) parameters and for a very short initial expansion of the contactor (0.3 or 0.6 ms), the model predicts that the spacecraft potential would reach values of the order of 1 kV. A 0.8-ms argon contactor expansion leads to 2–3 kV. (Note also that a longer contactor expansion decreases the peak spacecraft potential.) This is much lower than the energy of a relativistic beam, implying that the beam would easily be emitted. Moreover, kilovolt potentials are normal on geosynchronous spacecraft. They typically do not present a threat to spacecraft operation, but the spacecraft platform must be designed to avoid differential charging and the risk of electrostatic discharges.

Acknowledgments
The data used for the figures of the paper is supplied as supporting information. This work was funded by the Laboratory Directed Research and Development program (LDRD), under the auspices of the National Nuclear Security Administration of the U.S. Department of Energy by Los Alamos National Laboratory, operated by Los Alamos National Security LLC under contract DE-AC52-06NA25396. This research used resources provided by the Los Alamos National Laboratory Institutional Computing Program. J. E. B. was funded by the NASA magnetospheric GI program, the NASA Geospace SRT program, and by the NASA LWS TRT program. Resources supporting this work were provided by the Los Alamos National Laboratory Institutional Computing Program.

References

Akimov, P. V., Schamel, H., Kolinsky, H., Ender, A. Y., & Kuznetsov, V. I. (2001). The true nature of space-charge-limited currents in electron vacuum diodes: A Lagrangian revision with corrections. *Physics of Plasmas*, *8*, 3788–3798.

Bell, I. C., Leon, O., Miars, G. C., & Gilchrist, B. E. (2017). Experimental investigation of electron collection by rectangular cuboid probes in a high-speed plasma. *IEEE Transactions on Plasma Sciences*, *45*(7), 1788–1802.

Borovsky, J. E., McComas, D. J., Thomsen, M. F., Burch, J. L., Cravens, J., Pollock, C. J., et al. (2000). Magnetosphere-Ionosphere Observatory (MIO): A multisatellite mission designed to solve the problem of what generates auroral arcs. *Eos, Transactions American Geophysical Union*, *79*(45), F744.

Child, C. D. (1911). Discharge from hot CaO. *Physical Review*, *32*, 492–511.

Cohen, H. A., Adamo, R. C., Aggson, T., Chesley, A. L., Damron, D. M. C. S. A., Delorey, D. E., et al. (1980). P78-2 satellite and payload responses to electron beam operations on March 30, 1979. In *Proceeding of the Third Spacecraft Charging and Technology Conference* (pp. 509–559). Colorado Springs, CO: U.S. Air Force Academy.

Comfort, R. H., Moore, T. E., Craven, P. D., Pollock, C. J., Mozer, F. S., & Williamson, W. S. (1998). Spacecraft potential control by the Plasma Source Instrument on the POLAR satellite. *Journal of Spacecraft and Rockets*, *35*, 845–849.

Delzanno, G. L., Borovsky, J. E., Thomsen, M. F., Gilchrist, B. E., & Sanchez, E. (2016). Can an electron gun solve the outstanding problem of magnetosphere-ionosphere connectivity. *Journal of Geophysical Research: Space Physics*, *121*, 6769–6773. https://doi.org/10.1002/2016JA022728

Delzanno, G. L., Borovsky, J. E., Thomsen, M. F., & Moulton, J. D. (2015a). Future beam experiments in the magnetosphere with plasma contactors: How do we get the charge off the spacecraft? *Journal of Geophysical Research: Space Physics*, *120*, 3647–3664. https://doi.org/10.1002/2014JA020608

Delzanno, G. L., Borovsky, J. E., Thomsen, M. F., & Moulton, J. D. (2015b). Future beam experiments in the magnetosphere with plasma contactors: The electron collection and ion emission routes. *Journal of Geophysical Research: Space Physics*, *120*, 3588–3602. https://doi.org/10.1002/2014JA020683

Delzanno, G. L., Camporeale, E., Moulton, J. D., & Borovsky, J. E. (2013). E. A. MacDonald, and M. F. Thomsen CPIC: A curvilinear particle-in-cell code for plasma-material interaction studies. *IEEE Transactions on Plasma Sciences*, *41*(12), 3577–3587.

Delzanno, G. L., & Tang, X.-Z. (2016). Dust-plasma interaction: A review of dust charging theory and simulation. In G. Colonna & A. D'Angola (Eds.), *Plasma modeling: Methods and applications*, IOP Plasma Physics Series (pp. 13.1–13.26). Bristol, UK: IOP Publishing.

Dors, E. E., MacDonald, E. A., Kepko, L. E., Borovsky, J. E., Reeves, G. D., Delzanno, G. L., et al. (2017). CONNEX: Concept to connect magnetospheric physical processes to ionospheric phenomena. In *Active Experiments in Space: Past, Present and Future Workshop*. Sante Fe, NM.

Gilchrist, B. E., Banks, P. M., Neubert, T., Williamson, P. R., Myers, N. B., Raitt, W. J., & Sasaki, S. (1990). Electron collection enhancement arising from neutral gas jets on a charged vehicle in the ionosphere. *Journal of Geophysical Research*, *95*, 2469–2475.

Gussenhoven, M. S., Cohen, H. A., Hardy, D. A., Burke, W. J., & Chesley, A. L. (1980). Analysis of ambient and beam particle characteristics during the ejection of an electron beam from a satellite in near-geosynchronous orbit on March 30, 1979. In *Proceeding of the Third Spacecraft Charging and Technology Conference* (pp. 642–664). Colorado Springs, CO: U.S. Air Force Academy.

Hallinan, T. J., Stenbaek-Nielsen, H. C., & Winckler, J. R. (1978). The Echo 4 Electron Beam Experiment: Television observation of artificial auroral streaks indicating strong beam interactions in the high-latitude magnetosphere. *Journal of Geophysical Research*, *83*, 3263–3272.

Hendrickson, R. A., McEntire, R. W., & Winckler, J. R. (1975). Echo 1: An experimental analysis of local effects and conjugate return echoes from an electron beam injected into the magnetosphere by a sounding rocket. *Planetary and Space Science*, *23*, 1431–1444.

Huang, C. Y., Burke, W. J., Hardy, D. A., Grough, M. P., Olsen, D. G., Gentile, L. C., et al. (1998). Cerenkov emissions of ion acoustic-like waves generated by electron beams emitted during TSS 1R. *Geophysical Research Letters*, *23*, 721–724.

Inan, U. S., Bell, T. F., Bortnik, J., & Albert, J. M. (2003). Controlled precipitation of radiation belt electrons. *Journal of Geophysical Research*, *108*, 1186. https://doi.org/10.1029/2002JA009580

Jaffe, G. (1944). On the currents carried by electrons of uniform initial velocity. *Physical Review*, *65*(3–4), 91–98.

Kameyama, I., & Wilbur, P. J. (2000). Measurements of ions from high-current hollow cathodes using electrostatic energy analyzer. *Journal of Propulsion and Power*, *16*(3), 529–535.

Katz, I., Barfield, J. N., Burch, J. L., Marshall, J. A., Gibson, W. C., Neubert, T., et al. (1994). Interactions between the space experiments with particle plasma contactor and the ionosphere. *Journal of Spacecraft and Rockets*, *31*, 1079–1084.

Kelley, C. T. (1995). *Iterative methods for linear and nonlinear equations*. Philadelphia: Society for Industrial and Applied Mathematics.

Lavergnat, J. (1982). The French-Soviet experiments ARAKS: Main results. In B. Grandal (Ed.), *Artificial particle beams in space plasma studies* (pp. 87–100). Boston, MA: Springer US.

MacDonald, E. A., Borovsky, J. E., Larsen, B., & Dors, E. (2012). A science mission concept to actively probe magnetosphere-ionosphere coupling, Decadal Survey in Solar and Space Physics papers.

Meierbachtol, C. S., Svyatskiy, D., Delzanno, G. L., Vernon, L. J., & Moulton, J. D. (2017). An electrostatic particle-in-cell code on multi-block structured meshes. *Journal of Computational Physics*, *350*, 796–823.

Miars, G., Leon, O., Gilchrist, B. E., Delzanno, G. L., Lucco Castello, F., & Borovsky, J. E. (2017). Ion emission experiments enabling electron beam emission in tenuous plasmas. In *Active Experiments in Space: Past, Present and Future Workshop*. Sante Fe, NM.

Myers, N. B., Raitt, W. J., White, A. B., Banks, P. M., Gilchrist, B. E., & Sasaki, S. (1990). Vehicle charging effects during electron beam emission from the CHARGE-2 experiment. *Journal of Spacecraft and Rockets*, *27*, 25–37.

National Research Council (2012). *Solar and space physics: A science for a technological society*. Washington DC: National Academies Press.

Nemzek, R. J., Malcolm, P. R., & Winckler, J. R. (1992). Comparison of Echo 7 field line length measurements to magnetospheric model predictions. *Journal of Geophysical Research*, *97*, 1279–1287.

Nemzek, R. J., & Winckler, J. R. (1991). Electron beam sounding rocket experiments for probing the distant magnetosphere. *Physical Review Letters*, *67*, 987–990.

Neubert, T., & Banks, P. M. (1992). Recent results from studies of electron beam phenomena in space plasmas. *Planetary and Space Science*, *40*(2/3), 153–183.

Neubert, T., Burch, J. L., & Mende, S. B. (1995). The SEPAC artificial aurora. *Geophysical Research Letters*, *22*(18), 2469–2472.

Olsen, R. C. (1985). Experiments in charge control at geosynchronous orbit—ATS-5 and ATS-6. *Journal of Spacecraft and Rockets*, *22*, 254–264.

Pellat, R., & Sagdeev, R. Z. (1980). Concluding remarks on the ARAKS experiments. *Annales de Geophysique*, *36*, 443–446.

Prech, L., Nemecek, Z., Safrankova, J., & Omar, A. (2002). Actively produced high-energy electron bursts within the magnetosphere: The APEX project. *Annales de Geophysique*, *20*, 1529–1538.

Prech, L., Nemecek, Z., Safrankova, J., Simunek, J., Truhlik, V., & Shutte, N. M. (1995). Response of the electron energy distribution to an artificially emitted electron beam: APEX experiment. *Advances in Space Research*, *15*(12), 33–36.

Raitt, W. J., White, A. B., Fraser-Smith, A. C., Gilchrist, B. E., & Hallinan, T. J. (1995). VLF wave experiments in space using a modulated electron beam. *Journal of Spacecraft and Rockets*, *32*, 670–679.

Reeves, G. D., Banks, P. M., Neubert, T., Harker, K. J., & Gurnett, D. A. (1990). VLF wave emissions by pulsed and DC electron beams in space: 2. Analysis of Spacelab 2 results. *Journal of Geophysical Research*, *95*(A5), 6505.

Swanson, R. L., Steffen, J. E., & Winckler, J. R. (1986). The effect of strong pitch angle scattering on the use of artificial auroral streaks for echo detection—Echo 5. *Planetary and Space Science*, *34*, 411–419.

Tang, X.-Z., & Delzanno, G. L. (2014). Orbital-motion-limited theory of dust charging and plasma response. *Physics of Plasmas*, *21*(12), 123708.

Wilhelm, K., Bernstein, W., & Whalen, B. A. (1980). Study of electric fields parallel to the magnetic lines of force using artificially injected energetic electrons. *Geophysical Research Letters*, *7*, 117–120.

Winckler, J. R. (1980). The application of artificial electron beams to magnetospheric research. *Reviews of Geophysics*, *18*, 659–682.

Winckler, J. R. (1992). Controlled experiments in the Earth's magnetosphere with artificial electron beams. *Reviews of Modern Physics*, *64*, 859.

Zhulin, I. A., Kustov, A. V., Uspensky, M. V., & Miroshnikova, T. V. (1980). Radar observations of the overdense ionospheric ionization created by the artificial electron beam in the "Zarnitza-2" experiment. *Annales de Geophysique*, *36*, 313–318.